



OPEN

Remarkable plasma-resistance performance by nanocrystalline Y_2O_3 -MgO composite ceramics for semiconductor industry applications

Hyeon-Myeong Oh^{1,2}, Young-Jo Park^{1✉}, Ha-Neul Kim¹, Kundan Kumar¹, Jae-Woong Ko¹, Chae-Eon Lee¹ & Hyun-Kwun Lee²

Motivated by recent finding of crystallographic-orientation-dependent etching behavior of sintered ceramics, the plasma resistance of nanocrystalline Y_2O_3 -MgO composite ceramics (YM) was evaluated for the first time. We report a remarkably high plasma etching resistance of nanostructure YM surpassing the plasma resistance of commercially used transparent Y_2O_3 and $MgAl_2O_4$ ceramics. The pore-free YM ceramic with grain sizes of several hundred nm was fabricated by hot press sintering, enabling theoretical maximum densification at low temperature. The insoluble two components effectively suppressed the grain growth by mutual pinning. The engineering implication of the developed YM nanocomposite imparts enhanced mechanical reliability, better cost effectiveness with excellent plasma resistance property over their counterparts in plasma using semiconductor applications.

Plasma processes are widely used for the fabrication of state-of-the-art highly integrated semiconductor circuits¹. At present, high plasma power are inevitably required to control the dimensions of high-aspect-ratio contacts and deep-trench structures accurately (like in DRAM memory)^{1,2}. Ceramic components like focus rings and shower heads in a plasma-etching chamber are easily exposed to high-power plasma and generate contamination particles that cause a decrease in the integrated circuit (IC) manufacturing yield³⁻⁵. In order to protect the IC from particle contamination, ceramic coating is applied to the interior of the plasma chamber. Most commercially adopted plasma resistant materials are sintered oxide ceramics such as Al_2O_3 , quartz, and Y_2O_3 ⁶⁻¹⁰. Their high-temperature stability and chemical inertness found to be crucial in plasma shielding. Y_2O_3 is particularly more favorable than Al_2O_3 ¹¹⁻¹³ due to its low etching rate and high chemical stability against CF_4 plasma erosion^{8,14}. However, Y_2O_3 ceramic suffers from unnecessary grain growth at high temperature¹⁵, making Y_2O_3 a challenging system to obtain grain size in the sub-micron range—the coarser grain size results in poor mechanical property. The plasma resistance in ceramic is associated with the porosity, roughness, defect density, and mechanical property^{8,16}. Therefore, it is imperative to develop a system having a near theoretical density, fine grain size, low roughness, and high strength. Recently, Y_2O_3 -MgO composites have been fabricated to tackle the above-mentioned issues with Y_2O_3 ceramics. The composite has better mechanical strength than their individual oxides as the presence of one phase impedes the grain growth of the adjacent phase due to the pinning effect at the grain boundary¹⁷⁻¹⁹. At the same time, yttria is a rare earth compound, making it an expensive plasma shielding candidate. On the other hand, magnesium oxide is comparatively cheaper, making the composite of Y_2O_3 -MgO relatively economical with better plasma resistance property than the individual oxides.

To understand the erosion mechanism under CF_4 and NF_3 plasma, the erosion behavior of Y_2O_3 , Al_2O_3 and YF_3 have been reported^{14,20,21}. An oxide surface exposed to fluorocarbon plasma was initially fluorinated and then removed by a physical process combined with thermal cycling in wafer processing equipment²¹.

It is notable that the surface roughness controlled by microstructures such as the grain size and defects such as pores for both bulk parts and coating parts strongly affect the amount of etching^{16,22-24}. In an analogy to the

¹Engineering Ceramics Department, Korea Institute of Material Science, 797 Changwondaero, Changwon, Gyeongnam 51508, Republic of Korea. ²School of Advanced Materials Science and Engineering, Kumoh National Institute of Technology, Gumi, Gyeongbuk 39177, Republic of Korea. ✉email: yjpark87@kims.re.kr

Parameters	Condition
Source power, W	500
Bias power, W	100
Pressure, mTorr	10
CF ₄ :O ₂ , SCCM	40:10
Etching time, h	1, 2, 3

Table 1. Details of plasma etch conditions.

referred reports, engineers in the semiconductor manufacturing field realized that proper control of the microstructure is the first and foremost requirement for high-performance structural ceramics⁴. In a recent study, etching rate was found to be dependent on the crystallographic orientation²⁵. In other words, etching depth differs with different crystallographic plane for sintered polycrystalline ceramics. The authors are motivated by the above observation to determine the impact of grain anisotropic etching rate on ceramic surface roughness during plasma etching. Decrease in surface roughness eventually contributes in diminishing the particle generation problem during the plasma etching process¹⁴.

In this study, the plasma etching behavior of Y₂O₃-MgO composite ceramics (YM) featuring nano-sized grains was for the first time evaluated. A comparative study with the pore-free transparent Y₂O₃ and MgAl₂O₄ ceramics has been carried out. In our previous report²⁶, various transparent ceramics free from light-scattering pores, which also act as the origin and/or as a magnifier of the etching reaction, were proven to exhibit plasma resistance exceeding that of single-crystal sapphire. The nanostructured YM research has been pursued to its excellent mid-wavelength IR transmittance and reliable mechanical properties for use as hypersonic infrared windows, domes and eye-safe laser^{27–31}. The plasma resistance of YM composite ceramics has not yet been studied, although the monolithic forms of both Y₂O₃ and MgO have demonstrated excellent plasma resistance³². In this work, the characteristics of the plasma etching behavior were mainly discussed in terms of the surface properties and microstructural aspects.

Experimental procedure

Commercially available oxide powders of Y₂O₃ (99.9%, Rare Metallic, Japan), MgAl₂O₄ (99.9%, Baikowski, France) and MgO (99.99%, Sukgyung AT, Korea) were adopted as raw materials for the fabrication of monolithic Y₂O₃, monolithic MgAl₂O₄, and the composite YM ceramics. The details of the entire fabrication process of Y₂O₃ and MgAl₂O₄ are available in the literature^{33,34}. The process to fabricate YM composite is first 50:50 vol% of Y₂O₃ and MgO powders were mixed via ball milling and dried to evaporate milling fluid. The powder mixtures are uni-axially pressed in steel mold and then the green compacts were sintered by hot-pressing at 1300°C for 1 h under 40 MPa of pressure to reach nearly full theoretical density. After sintering, all samples were polished and masked on part of the top surface with polyimide tape to evaluate the etching properties. The thus-prepared nearly pore-free transparent ceramics were exposed to plasma using inductively coupled plasma. The details of the conditions used for plasma etching are listed in Table 1.

The density of the ceramic samples was determined by the Archimedes method. The theoretical density of the Y₂O₃, MgAl₂O₄ and YM ceramics were 5.031, 3.58, and 4.30 g/cm³, respectively. The crystal structure of sintered specimens was identified by X-ray diffraction (XRD; D/Mas 2500, Rigaku, Japan). The etching depth was measured by a surface profiler (DXT-A, Bruker, USA). The surface roughness and morphology were examined by the atomic force microscopy (XE-100, Park systems, Korea) and scanning electron microscopy (SU8230, Hitachi, Japan), respectively. The thermal diffusivity and heat capacity were measured by the laser flash analyzer (LFA 467, NETZSCH, Germany) and then the thermal conductivity (*k*) was calculated by following equation:

$$k = \alpha \cdot \rho \cdot C_p$$

where α , ρ and C_p is the thermal diffusivity, density and heat capacity, respectively. The microhardness was measured by indentation method (HM, Mitutoyo, Japan) and the fracture toughness was determined by the Anstis Eq.³⁵.

Results and discussion

Figure 1 shows the XRD patterns of sintered samples. The XRD peaks of YM composite have been indexed with the cubic Y₂O₃ (JCPDS 41-1105) and MgO (JCPDS 45-0946). No extra peak was noted in any sintered specimen, which confirms the phase purity of the samples.

The measured mass loss and etching depth of the ceramic specimens as a function of the plasma etching time are plotted in Fig. 2. With an increase in the plasma exposure time, both mass loss and etching depth monotonically increased for all specimens. The inversion of the magnitude of the mass loss and etching depth between Y₂O₃ and MgAl₂O₄ can be understood by considering the density differences, which were 5.031 g/cm³ for Y₂O₃ and 3.58 g/cm³ for MgAl₂O₄. Unlike the result of a medium level of mass loss, MgAl₂O₄ showed the deepest etching depth at all etching times. This tendency was noted to be similar to the earlier work²⁶ and herein, based on the mass loss and etching depth with Y₂O₃ and MgAl₂O₄ ceramics, particle contamination caused by the Y₂O₃ ceramics is postulated to be more reducible than that by MgAl₂O₄ ceramics, but further work is necessary for sufficient clarification. It is known that the etching depth of sintered polycrystalline Y₂O₃ is roughly half that

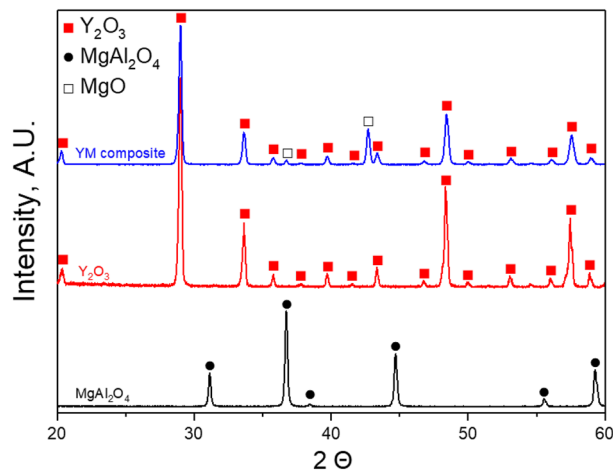


Figure 1. XRD patterns of YM composite, Y_2O_3 and $MgAl_2O_4$ ceramics.

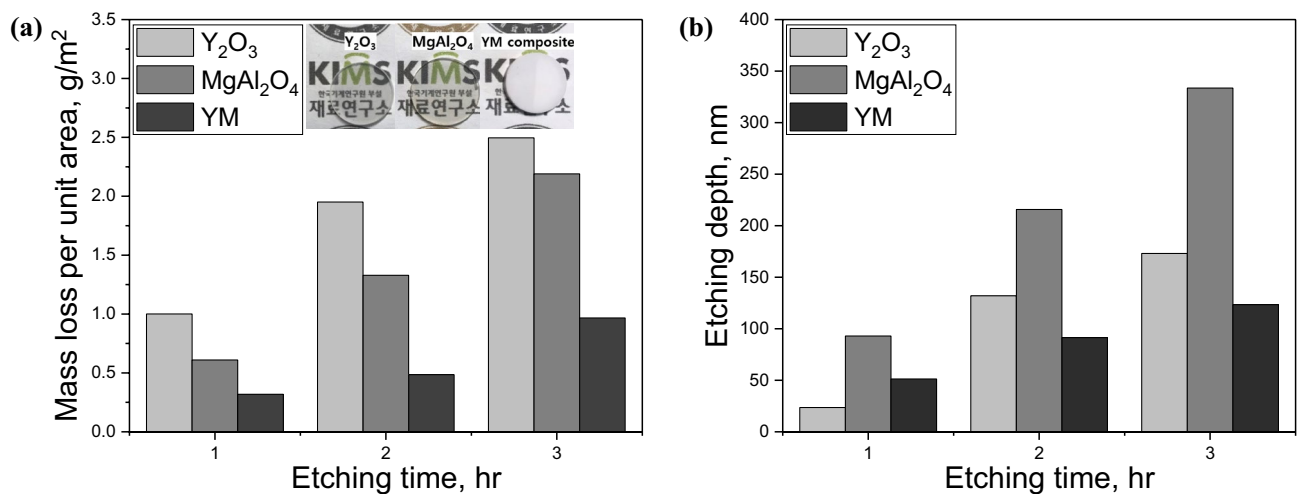


Figure 2. The measurement of (a) mass loss and (b) etching depth; the corresponding ceramic specimens after plasma etching are shown in the inset of Fig. (a) of which right half of each specimen was masked.

of single-crystal sapphire^{20,32}, while a previous report by the authors using pore-free transparent Y_2O_3 found best-ever results with a record low 20% etching depth compared to that of sapphire²⁶. It is surprising that the developed YM showed an even lower etching depth compared to that of transparent-grade Y_2O_3 , which will be discussed later with the results of microstructural analysis of the etched surface morphology. The images in the inset of Fig. 2(a) were taken after plasma etching, where the right half of each specimen was masked. For visible wavelength both monolith Y_2O_3 and $MgAl_2O_4$ are transparent, while YM is opaque owing to scattering caused not by pores but mismatch in refractive index between Y_2O_3 and MgO. Meanwhile, the evaluation of plasma-resistance remains both unclear and controversial^{4,36}. Accordingly, another way to characterize the etching behavior is to profile the etched. These results are presented in Figs. 3 and 4.

Figure 3 depicts AFM images of the etched surface profiling results. Topographical features after etching were clearly different in the three samples. The Y_2O_3 and YM ceramics tended to be homogeneously eroded by plasma exposure, resulting in an extremely smooth surface with $R_a = 4.0$ and 2.3 nm, respectively. On the other hand, the surface of $MgAl_2O_4$ was deeply eroded and, relatively rough; i.e., $R_a = 6.6$ nm. Generally, the surface roughness of conventional ceramics after plasma etching is reported to have a large range, from 100 nm to several microns, and these results have mainly been attributed to residual pores in the ceramics^{4,8,20}. For transparent ceramics having nearly pore-free microstructures, smooth erosion (plateau-like surface morphology) was found to be possible without selective erosion caused by ion bombardment around the pores^{4,25,26}. Given that the R_a value of the as-polished surface was under 2 nm, the AFM images in Fig. 3(c) reveal that the etched surface of YM was extremely smooth ($R_a = 2.3$ nm). Min et al. demonstrated that the surface roughness levels of transparent Y_2O_3 , $MgAl_2O_4$ and sapphire were 9.0, 10.3 and 27.0 nm, respectively, under etching conditions identical to those in this study²⁶. Kim et al. reported that the surface flatness during plasma etching played a critical role in reducing the generation of particles; it was noted that either the particles remained inside the chamber or were pumped

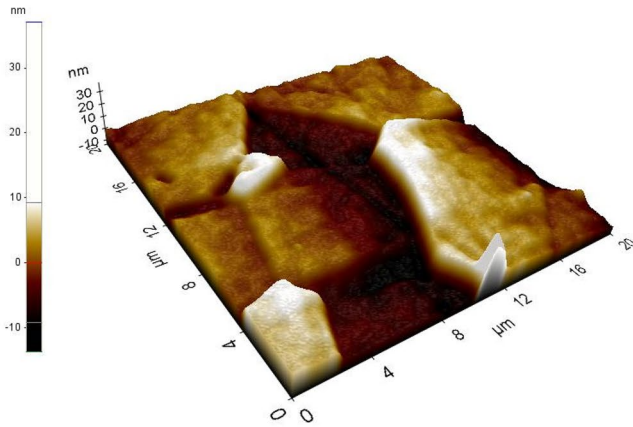
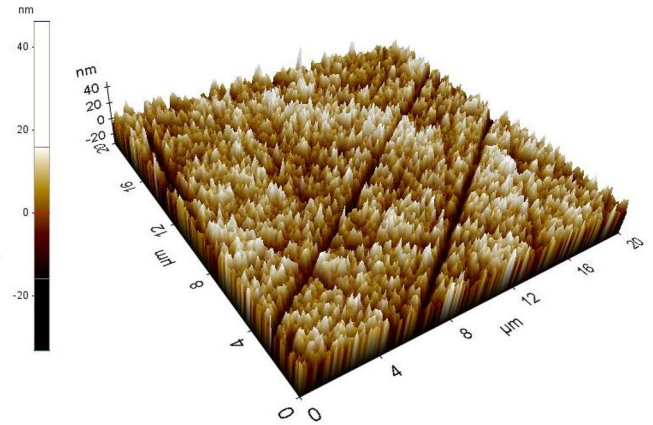
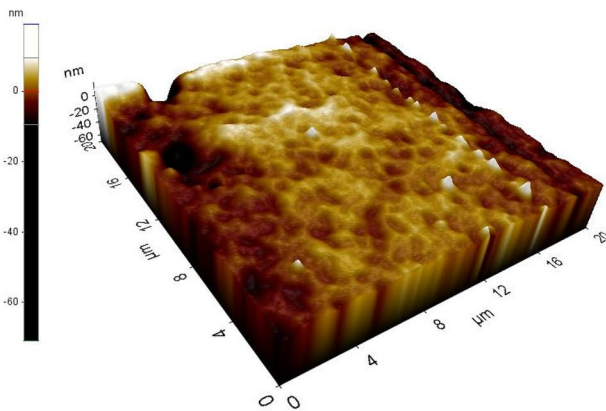
(a) $R_a = 4.0 \text{ nm}$, $G_{\text{avg.}} = 13 \text{ }\mu\text{m}$ (b) $R_a = 6.6 \text{ nm}$, $G_{\text{avg.}} = 1 \text{ }\mu\text{m}$ (c) $R_a = 2.3 \text{ nm}$, $G_{\text{avg.}} = 0.3 \text{ }\mu\text{m}$ 

Figure 3. AFM images of plasma etched surface of (a) Y_2O_3 , (b) MgAl_2O_4 and (c) YM.

out²¹. With an increase in the surface roughness, the condensed particle size simultaneously increased and the particles accumulated at the edge without being pumped out. The remaining large particles in the chamber may attach to the wafers, resulting in current shorts in integrated circuits³⁷. From this point of view, YM ceramics yielding the most smoothly etched surface is expected to be used to create promising plasma-resistant materials, leading to reduced particulate contamination. Furthermore, in an atmosphere of fluorine-based plasma, the chemical reaction of Y_2O_3 and MgO are YF_3 and MgF_2 , respectively. Their Gibbs free energy was estimated as -747 and -517 kJ/mol ^{38,39}. Therefore, a higher fluorine-plasma stability of MgO can explain a higher plasma resistance of YM composites than that of Y_2O_3 ceramics.

In order to elucidate the mechanism of the smooth surface roughness of the as-etched YM ceramics, the microstructural features of the Y_2O_3 and the YM ceramics were compared, as shown in Fig. 4. The grain sizes of the Y_2O_3 and YM were approximately $13 \text{ }\mu\text{m}$ and 300 nm , respectively. Clearly, the etching depth of the coarser Y_2O_3 grain appears to differ depending on each grain, as shown in Fig. 4(a). This phenomenon can be explained by the different plasma etching behaviors with respect to the grain orientation in polycrystalline Y_2O_3 ceramics²⁵. In contrast, the fine-grained microstructure of polycrystalline YM ceramics presented different etching behavior, as shown in Fig. 4(b). The schematics of the etched surface morphology in Fig. 4(c) and (d) specifically explain this. Based on the orientation-dependent erosion mechanism demonstrated by Kindelmann et al.²⁵, each coarse Y_2O_3 grain started to erode specifically on certain crystal planes, such as the (001) or (011) plane, resulting in higher surface roughness and deeper etching depths relative to the fine-grained YM ceramics. That is, the etching speed is always rate-controlled by the subsequently emerging slow-etch-rate oriented Y_2O_3 grains upon the etching away of both the fast-etch-rate Y_2O_3 grains and all MgO upper grains. Therefore, the greater plasma resistance of YM over Y_2O_3 ceramics is primarily considered to originate from the effect of nano-sized grains, as smaller grain size is effective during exposure with a slow etch rate of Y_2O_3 grains on the surface. As for the monolith Y_2O_3 it is postulated that etch-rate might decrease with decreasing grain size by the same analogy. It should be emphasized that the theory of ceramic processing on making the composite between two insoluble components (Y_2O_3 and MgO) was successfully utilized to fabricate pore-free nano-sized grain microstructure.

Moreover, given that physical and chemical etching simultaneously occur during plasma etching⁴⁰, another possible reason for the high plasma-resistance of YM ceramics is the higher mechanical reliability compared

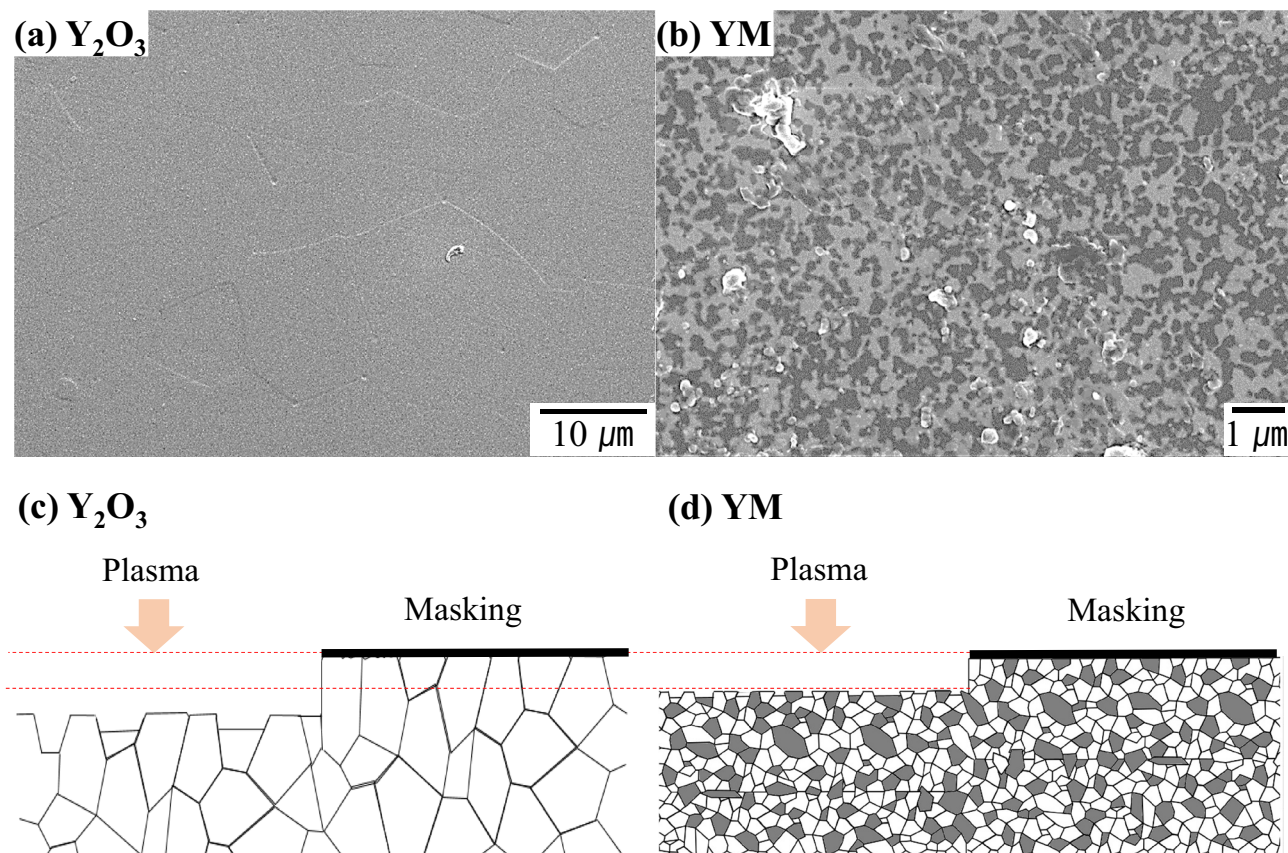


Figure 4. SEM and schematic images of plasma etched surface of (a, c) Y_2O_3 and (b, d) YM; (bright grain: Y_2O_3 , dark grain: MgO).

	Young's Modulus (GPa)	Microhardness (HV5, GPa)	Fracture Toughness (K_{IC} , $\text{MPa}\cdot\text{m}^{1/2}$)	Thermal conductivity (W/mK)
Y_2O_3	180 ⁴¹	7.6	2.0 ± 0.1	5.6
MgAl_2O_4	295 ⁴²	14.0	2.5 ± 0.1	15.9
YM	230 ⁴¹	9.9	3.0 ± 0.3	15.3

Table 2. Mechanical and thermal properties of specimens.

to Y_2O_3 and MgAl_2O_4 ⁴¹. Young's modulus of materials which stands for the inherent physical property are in the order of $\text{MgAl}_2\text{O}_4 > \text{YM} > \text{Y}_2\text{O}_3$ as shown in Table 2. The results of mechanical and thermal properties of specimens indicate that the inherently inferior physical properties of Y_2O_3 ceramics can be overcome by adopting YM composite with the highest fracture toughness and thermal conductivity. Kasashima et al. also reported a newly developed ceramic composite that showed enhanced plasma resistance given its improved mechanical properties and after an adjustment of the electrical resistivity³². The crucial microstructural aspects pertaining to the high strength of YM ceramics are the nano-sized Y_2O_3 and MgO grains, combining both suppressed grain growth and reaches full densification.

Conclusion

A nanocrystalline YM composite have been mainly studied to focus on its excellent IR transmittance and mechanical properties so far. The results here shed light for the first time on the feasibility of applying YM composite to parts requiring plasma resistance in the semiconductor processing industry. Specifically, the YM composite exhibited superior plasma resistance, including both a lower etching rate and smoother as-etched surface roughness relative of the transparent Y_2O_3 and Mg-spinel ceramic; originating from the effect of nano-sized grains with very carefully controlled microstructural defects, i.e., residual pores. Therefore, this novel trial with the YM composite for use in plasma environments is believed to set an important milestone to mitigate the particulate contamination issue in the semiconductor industry.

Received: 1 February 2021; Accepted: 23 April 2021
Published online: 13 May 2021

References

- Abe, H., Yoneda, M. & Fujiwara, N. Developments of plasma etching technology for fabricating semiconductor devices. *Jpn. J. Appl. Phys.* **47**, 1435 (2008).
- Andricacos, P. C., Uzoh, C., Dukovic, J. O., Horkans, J. & Deligianni, H. Damascene copper electroplating for chip interconnections. *IBM J. Res. Dev.* **42**, 567–574 (1998).
- Ito, N. *et al.* Reduction of particle contamination in plasma-etching equipment by dehydration of chamber wall. *Jpn. J. Appl. Phys.* **47**, 3630 (2008).
- Kim, D.-M. *et al.* Effects of artificial pores and purity on the erosion behaviors of polycrystalline Al₂O₃ ceramics under fluorine plasma. *J. Ceram. Soc. Jpn.* **117**, 863–867 (2009).
- Kitamura, J., Tang, Z., Mizuno, H., Sato, K. & Burgess, A. Structural, mechanical and erosion properties of yttrium oxide coatings by axial suspension plasma spraying for electronics applications. *J. Therm. Spray Technol.* **20**, 170–185 (2011).
- Bradley, J., Ay, F., Wörhoff, K. & Pollnau, M. Fabrication of low-loss channel waveguides in Al₂O₃ and Y₂O₃ layers by inductively coupled plasma reactive ion etching. *Appl. Phys. B* **89**, 311–318 (2007).
- Choi, K.-Y., Oh, Y.-S., Kim, S. & Lee, S.-M. High erosion resistant Y₂O₃-carbon electroconductive composite under the fluorocarbon plasma. *Ceram. Int.* **39**, 1209–1214 (2013).
- Iwasawa, J., Nishimizu, R., Tokita, M., Kiyohara, M. & Uematsu, K. Plasma-resistant dense yttrium oxide film prepared by aerosol deposition process. *J. Am. Ceram. Soc.* **90**, 2327–2332 (2007).
- Oh, H.-M., Park, Y.-J., Kim, H.-N., Ko, J.-W. & Lee, H.-K. Effect of powder milling routes on the sinterability and optical properties of transparent Y₂O₃ ceramics. *J. Eur. Ceram. Soc.* **41**, 775–780 (2020).
- Oh, H.-M., Park, Y.-J., Kim, H.-N., Ko, J.-W. & Lee, H.-K. Effect of milling ball size on the densification and optical properties of transparent Y₂O₃ ceramics. *Ceram. Int.* **12**, 1699 (2020).
- Cao, Y.-C. *et al.* Plasma etching behavior of Y₂O₃ ceramics: comparative study with Al₂O₃. *Appl. Surf. Sci.* **366**, 304–309 (2016).
- Wang, W.-K., Lin, Y.-X. & Xu, Y.-J. Structural and fluorine plasma etching behavior of sputter-deposition yttrium fluoride film. *Nanomaterials* **8**, 936 (2018).
- Lee, H.-K., Cho, K.-S. & Kim, M.-Y. Processing of plasma resistant alumina ceramics. *J. Korean Ceram. Soc.* **46**, 385–391 (2009).
- Song, J.-B., Kim, J.-T., Oh, S.-G. & Yun, J.-Y. Contamination particles and plasma etching behavior of atmospheric plasma sprayed Y₂O₃ and YF₃ coatings under NF₃ plasma. *Coatings* **9**, 102 (2019).
- Alhaji, A., Razavi, R. S., Ghasemi, A. & Loghman-Estarki, M. R. Modification of Pechini sol-gel process for the synthesis of MgO-Y₂O₃ composite nanopowder using sucrose-mediated technique. *Ceram. Int.* **43**, 2541–2548. <https://doi.org/10.1016/j.ceramint.2016.11.057> (2017).
- Zhao, D., Wang, C., Chen, Y. & Wang, Y. Phase composition, structural, and plasma erosion properties of ceramic coating prepared by suspension plasma spraying. *Int. J. Appl. Ceram. Technol.* **15**, 1388–1396 (2018).
- Muoto, C. K., Jordan, E. H., Gell, M. & Aindow, M. Effects of precursor chemistry on the structural characteristics of Y₂O₃-MgO nanocomposites synthesized by a combined sol-gel/thermal decomposition route. *J. Am. Ceram. Soc.* **94**, 372–381 (2011).
- Stefanik, T., Gentilman, R. & Hogan, P. in *Window and Dome Technologies and Materials X*. 65450A (International Society for Optics and Photonics).
- Huang, L., Yao, W., Liu, J., Mukherjee, A. K. & Schoenung, J. M. Spark plasma sintering and mechanical behavior of magnesia-yttria (50:50 vol.%) nanocomposites. *Scripta Mater.* **75**, 18–21 (2014).
- Kasashima, Y., Tabaru, T., Matsuda, O. & Motomura, T. Investigation of the relationship between plasma etching characteristics and microstructures of alumina ceramics for chamber parts. *Jpn. J. Appl. Phys.* **58**, 41001 (2019).
- Kim, D.-M. *et al.* Relative sputtering rates of oxides and fluorides of aluminum and yttrium. *Surf. Coat. Technol.* **309**, 694–697 (2017).
- Lee, B.-K. *et al.* Microstructure and properties of yttria film prepared by aerosol deposition. *J. Korean Ceram. Soc.* **46**, 441–446 (2009).
- Kobayashi, Y. Current status and needs in the future of ceramics used for semiconductor production equipment. *Osaka Japan* **17**, 115 (2005).
- Kim, D.-M. *et al.* The erosion behaviors of Y₂O₃ and YF₃ coatings under fluorocarbon plasma. *Thin Solid Films* **519**, 6698–6702 (2011).
- Kindelmann, M. *et al.* Erosion behavior of Y₂O₃ in fluorine-based etching plasmas: Orientation dependency and reaction layer formation. *J. Am. Ceram. Soc.* **15**, 6763 (2020).
- Min, J.-H. *et al.* Plasma etching properties of various transparent ceramics. *Ceram. Int.* **46**, 2895–2900 (2020).
- Liu, L., Morita, K., Suzuki, T. S. & Kim, B.-N. Synthesis of highly-infrared transparent Y₂O₃-MgO nanocomposites by colloidal technique and SPS. *Ceram. Int.* **15**, 130 (2020).
- Yang, S.-M. *et al.* Study on carbon contamination and carboxylate group formation in Y₂O₃-MgO nanocomposites fabricated by spark plasma sintering. *J. Eur. Ceram. Soc.* **40**, 847–851 (2020).
- Ma, H. J., Kong, J. H. & Kim, D. K. Insight into the scavenger effect of LiF on extinction of a carboxylate group for mid-infrared transparent Y₂O₃-MgO nanocomposite. *Scripta Mater.* **187**, 37–42 (2020).
- Ma, H. J., Jung, W. K., Park, Y. & Kim, D. K. A novel approach of an infrared transparent Er: Y₂O₃-MgO nanocomposite for eye-safe laser ceramics. *J. Mater. Chem. C* **6**, 11096–11103 (2018).
- Turky, A. O. *et al.* Achieving exceedingly constructional characterization of magnesia-yttria (MgO-Y₂O₃) nanocomposite obtained via oxalate precursor strategy. *Measurement* **150**, 106888 (2020).
- Kasashima, Y., Tsutsumi, K., Mitomi, S. & Uesugi, F. Development and evaluation of magnesium oxide-based ceramics for chamber parts in mass-production plasma etching equipment. *Jpn. J. Appl. Phys.* **56**, 06HC01 (2017).
- Zhu, L.-L. *et al.* Effects of ZrO₂-La₂O₃ co-addition on the microstructural and optical properties of transparent Y₂O₃ ceramics. *Ceram. Int.* **43**, 8525–8530 (2017).
- Kim, H.-N. *et al.* Fabrication of transparent MgAl₂O₄ spinel via spray freeze drying of microfluidized slurry. *Ceram. Int.* **43**, 11312–11317 (2017).
- Anstis, G., Chantikul, P., Lawn, B. R. & Marshall, D. A critical evaluation of indentation techniques for measuring fracture toughness: I, direct crack measurements. *J. Am. Ceram. Soc.* **64**, 533–538 (1981).
- Weigel, C., Schulze, M., Gargouri, H. & Hoffmann, M. Deep etching of Zerodur glass ceramics in a fluorine-based plasma. *Microelectron. Eng.* **185**, 1–8 (2018).
- Jun, H.-S. Diffusive plasma Dechucking method for wafers to reduce falling dust particles. *Jpn. J. Appl. Phys.* **52**, 66203 (2013).
- Lieberman, M. A. & Lichtenberg, A. J. *Principles of plasma discharges and materials processing*. (Wiley, 2005).
- Liu, C., Ji, X., Zhang, P., Chen, Q. & Banks, C. E. An oxygen pumping anode for electro-winning aluminium. *Phys. Chem. Chem. Phys.* **15**, 6350–6354 (2013).
- Shamiryani, D., Baklanov, M., Claes, M., Boullart, W. & Paraschiv, V. Selective removal of high-k gate dielectrics. *Chem. Eng. Commun.* **196**, 1475–1535 (2009).
- Harris, D. C. *et al.* Properties of an Infrared-Transparent MgO: Y₂O₃ Nanocomposite. *J. Am. Ceram. Soc.* **96**, 3828–3835 (2013).
- Kim, J.-W. *et al.* Microstructural evolution and relevant mechanical properties of Al-rich transparent magnesium aluminate ceramics. *J. Eur. Ceram. Soc.* **40**, 3222–3234 (2020).

Acknowledgements

This work was supported by the National Research Foundation (NRF) of MSIT of Korea (No. NRF-2020M3H4A3106003).

Author contributions

All authors reviewed and proofread the manuscript. H.-M.O. and Y.-J.P. mainly wrote the main manuscript and prepared figures.

Competing interests

The authors declare no competing interests.

Additional information

Correspondence and requests for materials should be addressed to Y.-J.P.

Reprints and permissions information is available at www.nature.com/reprints.

Publisher's note Springer Nature remains neutral with regard to jurisdictional claims in published maps and institutional affiliations.



Open Access This article is licensed under a Creative Commons Attribution 4.0 International License, which permits use, sharing, adaptation, distribution and reproduction in any medium or format, as long as you give appropriate credit to the original author(s) and the source, provide a link to the Creative Commons licence, and indicate if changes were made. The images or other third party material in this article are included in the article's Creative Commons licence, unless indicated otherwise in a credit line to the material. If material is not included in the article's Creative Commons licence and your intended use is not permitted by statutory regulation or exceeds the permitted use, you will need to obtain permission directly from the copyright holder. To view a copy of this licence, visit <http://creativecommons.org/licenses/by/4.0/>.

© The Author(s) 2021